International Journal of Thermophysics, Vol. 23, No. 1, January 2002 (© 2002)

Characterization of Macromolecular Solutions by a Combined Static and Dynamic Light Scattering Technique[1]

S. V. Kazakov,[2, 3] I. Yu. Galaev,[2] and Bo Mattiasson[2, 4]

The combination of quasi-elastic light scattering (LS) with integrated scattered intensity measurements in the same sample has been applied to study polymer and polymer–protein aqueous solutions. The molecular weight, the radius of gyration, and the second virial coefficient for thermosensitive polymer [poly(*N*-isopropylacrylamid)] solutions before and after precipitation transition have been obtained using Zimm plot calculations. The precipitation curve (intensity versus temperature dependence) for polymer solutions has been experimentally obtained using the light scattering setup. For the first time the static and dynamic LS properties of aqueous solutions of antibody–poly(methacrylic acid) and antibody–poly(acrylic acid) conjugates and solutions of their components [antibody, poly(methacrylic acid), and poly(acrylic acid)] at different pH values have been measured. In both cases the parallel comparison of the characteristic size variations allowed us to represent novel structural features of scattered particles (macromolecules, associates, aggregates, conjugates, colloidal particles) in studied systems.

KEY WORDS: aggregation; association; conjugate; cooperative interactions; light scattering; polymer; precipitation; protein.

1. INTRODUCTION

Light scattering (LS) is a highly informative method, and the combination of quasi-elastic LS and integrated scattered intensity measurements in the

[1] Paper presented at the Fourteenth Symposium on Thermophysical Properties, June 25–30, 2000, Boulder, Colorado, U.S.A.

[2] Department of Biotechnology, Center for Chemistry and Chemical Engineering, Lund University, P.O. Box 124, S-221 00 Lund, Sweden.

[3] Guest scientist from Faculty of Physics, Lomonosov Moscow State University, 119899 Moscow, Russia.

[4] To whom correspondence should be addressed. E-mail: Bo.Mattiasson@biotek.lu.se

0195-928X/02/0100-0161/0 © 2002 Plenum Publishing Corporation

same experimental setup increases the amount of information for the systems studied [1]. Recently, photon correlation spectroscopy (PCS) has become a popular technique for studying structural transformations in systems containing proteins, enzymes, polymers, and other macromolecular components [2, 3].

Table I presents parameters which can be calculated from the data of static and dynamic LS. The first row gives the formulas for concentration and angular dependences of static and dynamic Zimm plots. The second row presents the experimental parameters along with the limitations imposed on c and Θ using these expressions. The remaining parameters can be compared as equivalent sphere radii that are represented in the next row of Table I. From static LS one gets two effective sizes: radius of gyration, R_g, and thermodynamic radius, R_T, from dynamic LS—hydrodynamic radius, R_h. The magnitudes of these radii can differ from each other [4]. These differences result from the fact that they are physically differently defined. R_g is solely geometrically defined, but there are two types of interactions between particles in a solution of finite concentration: hydrodynamic and thermodynamic.

Table I. Six Quantities Obtained from the Static and Dynamic Zimm Plots

	Static	Dynamic
Formula	$Kc/R_\Theta(q,c) = (1+q^2R_g^2/3)/M_w + 2A_2c + 2A_3c^2 + \cdots$	$D(q,c) = D_0(1+Cq^2R_g^2+\cdots) \leftrightarrow (1+k_Dc+\cdots)$
Experimental conditions and parameters	$qR_g < 2$, $A_2M_wc < 0.5$ K is the optical constant, c is the concentration, R_Θ is the Rayleigh ratio, $q = (4\pi n_0/\lambda_0)\sin(\theta/2)$ is the magnitude of the scattering vector, n_0 is the refractive index of the solvent, λ_0 is the wavelength of the primarily beam in vacuum, Θ is the scattering angle, η is the viscosity of the solvent, T is the absolute temperature, and k_b is Boltzmann's constant	
Extracted molecular parameters	Weight-average molecular weight M_w (intercept) Z-average radius of gyration $R_g^2 \cdots \langle S^2\rangle_Z$ (slope at $c=0$) Second virial coefficient A_2 (slope at $q=0$)	Diffusion coefficient $D_0 = kT/6\pi\eta R_h$ (intercept) Architecture parameter CR_g^2 (slope at $c=0$) k_D (slope at $q=0$)
Equivalent sphere radii	R_g, the radius of gyration, is solely geometrically defined; $R_T = (3A_2M_w/16\pi N_A)^{1/3}$, the thermodynamically effective equivalent radius, is defined by domains of interaction between two macromolecules	$\langle d_h\rangle = k_bT/3\pi\eta D$, the hydrodynamic diameter, results from the interaction of macromolecules with the solvent

R_h characterizes hydrodynamic interactions and indicates how deeply a particle is drained by the solvent: a deep draining causes a reduction in R_h; on the other hand, if only shallow draining is possible, R_h can become much larger than R_g. The thermodynamic interactions (repulsion or attraction) are characterized by the thermodynamically effective equivalent sphere radius R_T, which is defined by the domains of interpenetration of two macromolecules or, in other words, by the excluded volume. Generalized ratios of these differently defined radii can be derived. The ratio $\rho = R_g/R_h$ compares the range of hydrodynamic interaction with the geometrical dimensions of the molecule and can be theoretically calculated for the selected structures. For example, for a homogeneous sphere ρ is less than unity, for microgels it can be less than 0.5, for random coil it changes from 1.5 to 2, depending on the polydispersity, solvent, and conditions, and for a rigid rod it is greater than 2. The ratio $V_T = R_T/R_h$ compares the range of thermodynamic interactions with that of hydrodynamic interactions. Experiments mostly demonstrate that the ratio is close to unity: this means that the thermodynamic and hydrodynamic interactions act over very similar distances.

Thus, it follows from analysis of Table I that a complete picture of structural features of scattered particles in solution can be obtained by parallel correlation of characteristic sizes which are the result of static and dynamic LS measurements in the same sample and under identical experimental conditions. We demonstrate these opportunities with the example of the application of the LS technique to the study of the precipitation of a well-known thermosensitive polymer, poly(*N*-isopropylacrylamide) (PNIPAM), determining the temperature of phase transition in aqueous solutions and measuring the molecular weight, radius of gyration, and second virial coefficient before and after the transition.

Moreover, in this paper we focus on the molecular and structural parameters of poly(methacrylic acid) (PMAA), poly(acrylic acid) (PAA), antibodies (Abs), and their conjugates with PMAA and PAA in aqueous solutions determined by static and dynamic LS. Particular attention is given to elucidation of the interdependence of the components affecting the association and aggregation of the conjugates.

Study of protein–polymer conjugates in which the role of protein is played by an Ab is of special interest. Despite the great variety of Abs, their molecules are structurally similar and characterized by virtually the same isoelectric point. To us, Ab–polymer systems are of particular interest for several reasons. (i) A study of the features of Ab–polymer conjugates and variation of their structure with pH is a prerequisite to understanding higher-order systems (e.g., complexes of two conjugates) [5, 6]. (ii) Investigation and recognition of the role of the constituents of the conjugates are

crucial for understanding their aggregation and precipitation. In turn, the control of association and aggregation processes in the multicomponent systems is essential for the development of bioseparation methods and specific assays. (iii) Protein–polymer complexes have been studied by many experimental methods [7, 8].

There is still a lot of theoretical and experimental problems hindering the acquisition of reliable data from PCS measurements. However, in the particular case of pronounced aggregation, the significant variations in macromolecular size of the associated species provide a straightforward interpretation of PCS results. To the best of our knowledge, aqueous solutions of Abs and, in particular, the behavior of Abs and their conjugates with polyelectrolytes in response to changes in pH have not been studied using the LS technique.

2. MEASUREMENTS

2.1. Specimens

Milli-Q water with $R \approx 18\ \mathrm{M\Omega \cdot cm}$ and 10 mM phosphate buffer, containing 0.1M NaCl, were used in all experiments. Monoclonal Abs from the 6C5 clone against inactivated rabbit muscle glyceraldehyde-3-phosphate dehydrogenase were raised in mice and characterized by their binding to native and inactivated forms of the enzyme [9]. The Ab concentration was determined by UV absorbance measured at 280 nm (E_{280} for 0.1% v/w was 1.5). The stock Ab solution, with an initial Ab concentration of $1.48\ \mathrm{mg \cdot ml^{-1}}$, was diluted to $0.74\ \mathrm{mg \cdot ml^{-1}}$ before LS measurements. The Ab isoelectric point (pI 5.95) was determined previously [11]. Synthesis of PMAA and PAA with a degree of polymerization of 1830 and 3200, respectively, is described elsewhere [5, 6].

The stock solution of PMAA was prepared with a concentration of $38.3\ \mathrm{mg \cdot ml^{-1}}$, diluted to $4.8\ \mathrm{mg \cdot ml^{-1}}$, and then filtered using a 0.2-μm Sartorius Minisart filter in the ∅10-mm sample cell. The initial pH of this sample was 5.0. The stock solution of PAA was prepared with a concentration of $2.9\ \mathrm{mg \cdot ml^{-1}}$, diluted to $0.091\ \mathrm{mg \cdot ml^{-1}}$, and then filtered using a 0.2-μm Sartorius Minisart filter in the ∅10-mm sample cell. The initial pH of this sample was 5.8.

Conjugates of PMAA and PAA with the Abs (Ab–PMAA and Ab–PAA) were synthesized by covalent binding using a procedure including water-soluble carbodiimide [5, 6]. The stock Ab–PMAA solution, with a concentration of $1\ \mathrm{mg \cdot ml^{-1}}$, was diluted four times and then filtered using a 0.2-μm Sartorius Minisart filter in the quartz ∅10-mm sample cells. The Ab–PAA solution, with a concentration of $0.85\ \mathrm{mg \cdot ml^{-1}}$, was filtered using

a 0.2-μm Sartorius Minisart filter in the quartz ∅10-mm sample cells. The pH of all solutions was adjusted by adding a corresponding amount of a 0.1*M* HCl solution or a 0.2*M* NaOH solution.

PNIPAM was synthesized by radical polymerization in an aqueous solution at room temperature using the redox pair ammonium persulfate–tetraethylene methylenediamine (TEMED) as the initiator and purified by three sequential reprecipitations at 40°C. For Zimm plot measurements (angular and concentration dependence of the excess Rayleigh ratio; see Table I), four aqueous solutions of PNIPAM with different concentrations (0.38, 0.29, 0.19, and 0.096 $mg \cdot ml^{-1}$) were prepared and filtered using a 0.2-μm Sartorius Minisart filter in the quartz ∅10-mm sample cells. The precipitation curve was obtained for the solution with a concentration of 0.019 $mg \cdot ml^{-1}$.

2.2. Light Scattering

LS measurements were done with a Malvern 4700c system. An argon ion laser (Uniphase 2213-75 SL) operating at a 488-nm wavelength and 30-mW output power was used as a light source. The scattering angle was varied from 30 to 150° in 13 steps. The spectrometer was calibrated with distilled water and toluene to make sure that the scattering intensity from water and toluene had no angular dependence in the angular range used.

Measurements of the angular and concentration dependence of the average scattering intensity of PNIPAM solutions lead to the weight-average molecular weight (M_w), the radius of gyration (R_g), and the second virial coefficient (A_2). The specific refractive index increment (dn/dc) of PNIPAM in water was evaluated as 0.165 and 0.170 $ml \cdot g^{-1}$, respectively, at 23 and 37°C.

All measurements of the solutions of PAA, PMAA, Ab, and their conjugates were performed at 25.0 ± 0.1°C. In static LS we used an angle scan with axes of inverse intensity vs q^2 to calculate the radius of gyration R_g:

$$I_{\Theta}^{-1}(q) \cong I_0^{-1}(1 + \tfrac{1}{3} R_g^2 q^2) \tag{1}$$

In this equation I_{Θ}^{-1} is the inverse scattering intensity at scattering angle Θ. The limit $qR_g < 2$ was fulfilled within the range of scattering angles for all systems studied.

The intensity–intensity time autocorrelation functions of the scattered intensity in the self-beating mode can be related to the normalized first-order electric field time correlation function $g^{(1)}(t, q)$ as

$$G^{(2)}(t) = \langle I(0)\, I(t) \rangle = B[1 + \beta\, |g^{(1)}(t, q)|^2] \tag{2}$$

where β is a parameter depending on the coherence of the detection, t is the delay time, and B is the measured baseline. The logarithmic correlation function can be expanded in a power series in terms of the delay time (cumulant analysis),

$$\ln g^{(1)}(t) = -\Gamma_1 t + (\Gamma_2/2!)\, t^2 - (\Gamma_3/3!)\, t^3 + \cdots \tag{3}$$

where Γ_1, Γ_2, etc., are the first, second, etc., cumulants. The first cumulant can be calculated by equilibrium statistical thermodynamics and, at low q, related to the apparent diffusion coefficient D: $\Gamma_1 = Dq^2$. The "Z-average particle size" can be found using the well-known Stokes–Einstein relationship, which is a definition for a hydrodynamically effective sphere diameter $\langle d_h \rangle$ (see Table I). If the sample is polydisperse, the value $2\Gamma_2/\Gamma_1^2 = \mathrm{PI}$, the polydispersity index (the width of the distribution), which is the dimensionless measure of the broadness of the distribution.

Dynamic measurements were performed as follows. The scattering angle was kept constant at 90°. The quality of measurement was checked over the signal-to-noise ratio and the range of the correlation function. The intensity autocorrelation function was collected in 128 channels and in a so-called far point, a special group of correlator channels pushed out in time by a special extension of the memory. The difference between the measured and the calculated baselines was taken into account. It was observed that the field–field correlation function is single-exponential for all samples studied. The particle size distribution and average particle size were obtained from the correlation function by fitting the data with cumulant analysis, using the PCS software program (Version 1.35) supplied by Malvern Instruments Ltd.

3. RESULTS AND DISCUSSION

3.1. Phase Transition of PNIPAM

It is known that the scattered intensity is proportional to the spatial fluctuations of concentrations $I \sim \langle \Delta c^2 \rangle$, and one can expect that this value will be more sensitive when approaching the cloud point of the polymer. We have used this fact for the determination of the temperature of the phase transition in aqueous solutions of the thermosensitive polymer PNIPAM (Fig. 1). A conformational random coil–globule transition for PNIPAM before the phase transition is well documented [12] in extremely diluted solutions. We have observed this effect for rather concentrated solutions.

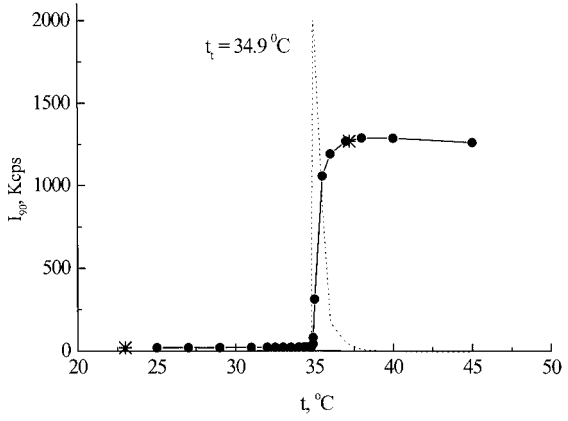

Fig. 1. Precipitation curve for aqueous solutions of PNIPAM measured by LS.

Static LS measurements (angular and concentration dependences) were carried out at 23 and 37°C, i.e., before and after the transition: points are indicated on the precipitation curve (Fig. 1). The typical Zimm plot calculated by Malvern Instruments Ltd. software is presented in Fig. 2. Table II lists the extracted parameters: M_w, R_g, and A_2. These data indicate that aggregates with a 60-fold higher molecular weight but two times lower size are formed after the transition. The aggregates exist in solution as a stable suspension. A significant decrease in the second virial coefficient corresponds to the solution under Θ conditions. The values of R_T before and

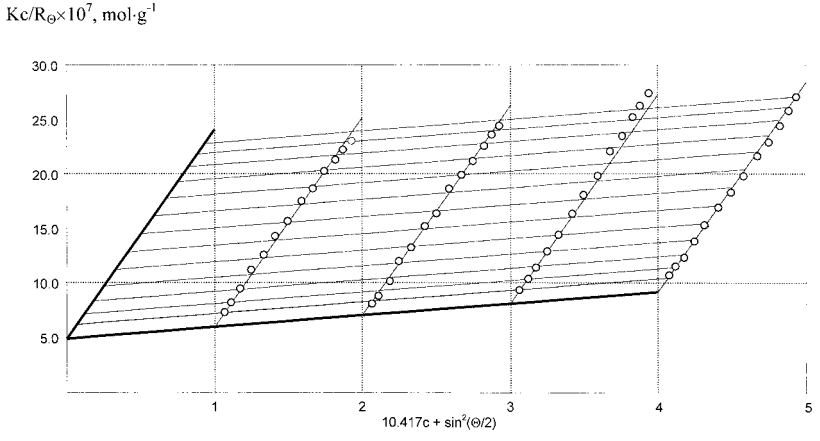

Fig. 2. Typical Zimm plot for the aqueous solution of PNIPAM at 23°C.

Table II. Zimm Plot Data for PNIPAM/Water Solutions at Different Temperatures

Temperature (°C)	$M_w \times 10^6$ ($g \cdot mol^{-1}$)	R_g (nm)	$A_2 \times 10^3$ ($mol \cdot ml \cdot g^{-2}$)	R_T (nm)	Structure
23	2.04	100	1.11	28	Random coil
37	126	50	1.33×10^{-3}	11.8	Aggregate of globules

after the phase transition, i.e., both for random coils and for aggregates of globules, indicate strong polymer–polymer interactions expressed in significant overlapping areas.

3.2. Characterization of Conjugates and Their Free Components

3.2.1. Polymers

The parameters for PMAA obtained by combined static and dynamic LS at different pH values are presented in Figs. 3 and 4 (PMAA). As expected, no aggregation or precipitation occurred over the whole pH range studied. However, polymer chains expanded cooperatively, forming a more homogeneous medium with increasing pH. The *Z*-average radius of gyration R_g increased sharply at pH > 5 (Fig. 3a; PMAA). The parameter $\langle d_h \rangle$ appeared to be less sensitive to the changes in scattering particle shape in this case (Fig. 4a; PMAA). The set of data on R_g and $\langle d_h \rangle$ obtained allows us to conclude that the PMAA chain expansion (increase in R_g) is accompanied by the retention of the domain sizes $\langle d_h \rangle$ of effective polymer–solvent interactions. Herein, numeric values of the ratio $2\langle R_g \rangle / \langle d_h \rangle$ varied in the range 1.75 to 2.5, which represents values typical for polymer molecules with a random coil structure under Θ conditions and in good solvents, respectively. The decrease in LS intensity (Fig. 3b; PMAA), which was proportional to the concentration fluctuations, indicated a more homogeneous state of cooperatively expanded polymer chains. On the other hand, it is obvious that a more compact form of polymer has to have fewer deviations in molecular size, and vice versa. This fact was reflected in the increase in PI at pH > 5 (Fig. 4b; PMAA).

The properties of PAA are expected to differ sharply from those of PMAA, although the only difference in the chemical structures of these polyacids consists of the methyl groups in the α position of the PMAA molecules [6, 10]. The data on static and dynamic LS measurements of PAA solutions presented in Figs. 3 and 4 (PAA) demonstrate no conformational transition of PAA molecules over the whole range of pH values studied (2.5 to 9), confirming that the hydrophobic interactions of methyl

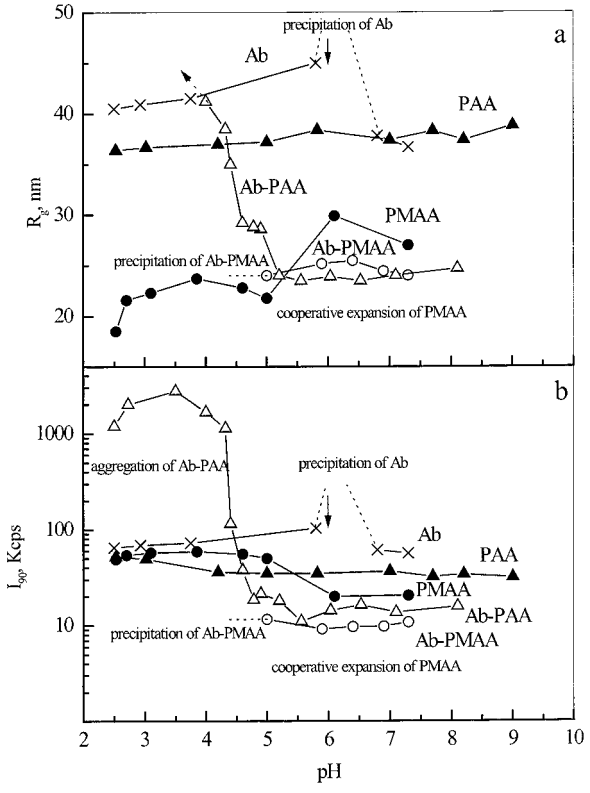

Fig. 3. pH dependences of (a) radius of gyration and (b) scattering intensity for solutions of free poly(methacrylic acid) (PMAA), poly(acrylic acid) (PAA), free antibodies (Ab), and Ab–PMAA and Ab–PAA conjugates. The solid arrow indicates the position of the determined isoelectric point for antibodies of the 6C5 clone. The dotted arrow indicates that calculations of the radius of gyration at a pH > 4 were not fulfilled for the solution of Ab–PAA conjugates.

groups in PMAA are responsible for the stability of the local compact structures in this polyacid molecule in acidic medium and for their cooperative expansion in neutral medium.

3.2.2. Antibody

The protein solubility decreases around the isoelectric point. In our experiments precipitation of Ab molecules was observed after the addition of 0.5*M* HCl when the pH changed from 6.8 to 5.9, in the region close to the p*I* of the antibodies (p*I* 5.95). The pH dependences of the radius of

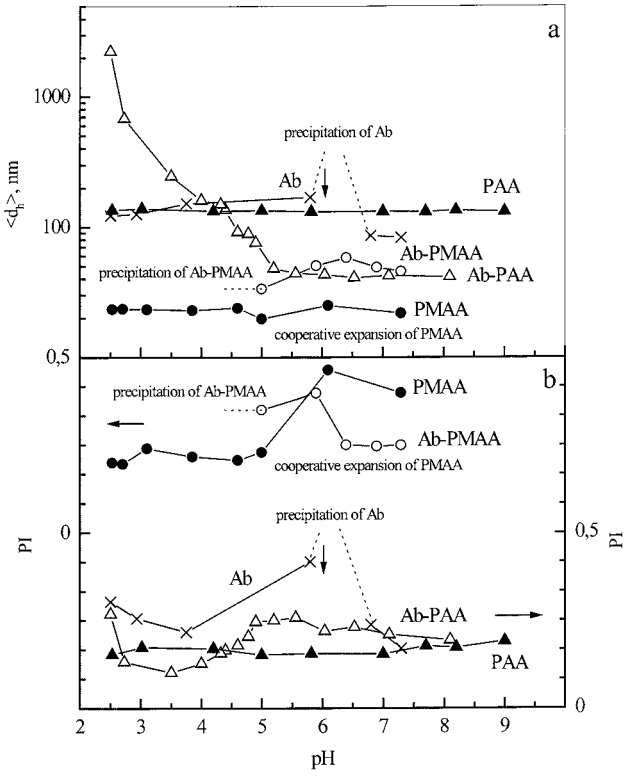

Fig. 4. pH dependences of (a) *Z*-average hydrodynamic diameter and (b) polydispersity index for solutions of free poly(methacrylic acid) (PMAA), poly(acrylic acid) (PAA), free antibodies (Ab), and Ab–PMAA and Ab–PAA conjugates. The solid arrow indicates the position of the determined isoelectric point for antibodies of the 6C5 clone.

gyration (a), LS intensity (b), hydrodynamic diameter (c), and polydispersity index (d) of antibodies are presented in Figs. 3 and 4. The precipitation at a pH of about 6.0 (shown by dotted lines in the figures) is accompanied by significant variations of the overall measured characteristics, indicating the pronounced association of Ab molecules. Further evidence of the association of free Abs could be derived from the comparison of their size with the size of the Ab–MAA conjugate.

3.2.3. Polymer–Protein Conjugates

The static and dynamic LS data for the Ab–PMAA conjugates indicated a shift of the precipitation transition for the Ab–PMAA conjugate to a more

acidic medium (pH ~ 4.8) compared to the solution of free Ab (pH ~ 6) (Figs. 3 and 4; Ab–PMAA).

The comparison of LS data for the Ab solution with the data for the solution of Ab–PMAA conjugates highlights the effect of PMAA on the ability of Abs to associate. The covalent attachment of charged polymers to Ab molecules prevents the latter from approaching each other and associating.

The next experimental fact obtained for the Ab–PMAA conjugate solution is a decrease in R_g (Fig. 3a; Ab–PMAA) and $\langle d_h \rangle$ (Fig. 4a; Ab–PMAA), as well as an increase in I_{90} (Fig. 3b; Ab–PMAA) and PI (Fig. 4b; Ab–PMAA) in the pH range 5 to 6, which precedes the precipitation of Ab–PMAA conjugates at pH ~ 4.8. These changes in LS parameters are directly connected with the cooperative shrinkage of PMAA polymer chains. Thus, there are strong grounds to believe that the compact conformation of PMAA in acidic media is mainly responsible for the observed precipitation of Ab–PMAA conjugates.

Some assumptions about the structure of the conjugates could be made from the comparison of the LS parameters of Ab–PMAA conjugates and free PMAA. In a neutral medium before precipitation, the R_g of conjugates (Fig. 3a; Ab–PMAA) is less than the corresponding size of cooperatively expanded coils of PMAA (Fig. 3a; PMAA). This fact testifies that a strong interaction between polymer chains and protein favors the compact arrangement of polymer chains around the protein globule. The geometrical size (R_g) of the conjugate decreased slightly in the pH interval 5 to 6, whereas the hydrodynamic size ($\langle d_h \rangle$) of the conjugate decreased more significantly, reflecting cooperative shrinkage of the polymer coil around the protein globule. At the same time, the $\langle d_h \rangle$ of the conjugate significantly exceeded the $\langle d_h \rangle$ of the free polymer. This indicates strongly that the protein globule gains an interaction of the conjugate with the molecules of the solvent. A hydrated shell is formed around the conjugate. The shell is penetrated by the polymer chain, and the thickness of the shell varies depending on the conformational state of the polymer.

To confirm this proposed structure of the polymer–protein conjugate, PAA, with a degree of polymerization significantly higher than that of PMAA, was selected for covalent attachment to Ab and formation of Ab–PAA conjugates. Contrary to PMAA, PAA has no α-methyl groups in polymer chains, and as a result, no conformational transformations were observed in the pH range studied (Figs. 3 and 4; PAA). Static and dynamic LS parameters of the Ab–PAA conjugate solution at different pH values are presented in Figs. 3 and 4 (Ab–PAA). There was no precipitation over the whole range of pH (2.5 to 8.0), but the behavior of all measured parameters was quite different in neutral (pH 4.8 to 8.0) and acidic (pH < 4.8) media.

In a neutral medium both the static and the dynamic characteristics hardly varied with pH. Again, the values of both R_g and $\langle d_h \rangle$ for Ab–PAA conjugates were less than the corresponding values for free Abs, indicating the ability of the polymer to prevent the association of protein molecules.

An increase in the average radius of gyration (Fig. 3a; Ab–PAA) and the average hydrodynamic diameter (Fig. 4a; Ab–PAA) of scattering particles was found in the acidic medium of the Ab–PAA conjugate solution. This fact, as well as the sharp increase in the scattering intensity (Fig. 3b; Ab–PAA) along with the initial decrease in the polydispersity index in the first stage (Fig. 4b; Ab–PAA), unambiguously testifies that the process of aggregation starts at a $pH < 4.8$. An increase in the opalescence of the solution was observed at a $pH < 4.8$, but the solution remained completely homogeneous, indicating no precipitation. Under a further decrease in pH, the elevation of $\langle d_h \rangle$ and I_{90} and the drop in PI slowed down in the pH range 3 to 4. Calculations of R_g using Eq. (1) were impossible in this range due to the strong asymmetry of the angular dependence of the scattering intensity. This is indicated by the dashed arrow in Fig. 3a (Ab–PAA). At a $pH < 3$ a sharp increase in $\langle d_h \rangle$ and PI occurred, probably because colloid particles of Ab–PAA conjugates started binding to each other. As a result, the decrease in scattering intensity at a $pH < 3$ (Fig. 3b; Ab–PAA) could be explained by a progressive influence of the multiple scattering. However, in this pH range, even under colloidal particle formation, the solution remains stable, homogeneous, and transparent, i.e., there is no precipitation. The particles are stabilized by electrostatic repulsion caused by the still sufficiently high charge density of the PAA coil even in acidic medium ($3 < pH < 4.8$) preventing the system from precipitation and/or a hydrated shell formed by water molecules bound to COOH groups of PAA via hydrogen bonds.

The average values of R_g (Fig. 3a; PAA) and $\langle d_h \rangle$ (Fig. 4a; PAA) for free PAA appear to be larger than the sizes of Ab–PAA conjugates (Figs. 3a and 4a; PAA) over the whole pH range (4.8 to 8.0). This could mean that, after attachment of the polymer to the protein, the former surrounds the surface of the Ab in a compact manner. A significant excess of the hydrodynamic radius over the radius of gyration indicates strong interactions of conjugate with solvent molecules. At the same time the characteristic dimensions of different conjugates appear to be close to each other despite the difference in the polymer chain lengths of PMAA and PAA attached.

4. CONCLUSIONS

The results presented clearly demonstrate that the combination of static and dynamic LS gives real perspectives in the analysis of the structural and

molecular characteristics of thermosensitive polymers, proteins, and polymer–protein complexes in solution, and their aggregation and precipitation near phase transitions. The comparison of physically different characteristic molecular dimensions (radius of gyration, thermodynamic radius, and hydrodynamic radius) along with other static and dynamic parameters (scattering intensity, PI) is a powerful tool for developing structural models of the macromolecular systems.

In particular, the results of our investigation of LS parameters for PMAA, PAA, Abs, and their conjugates with the polymers confirm that (a) the conformational compactness of the polymer plays a crucial role in the process of precipitation; (b) the attached polymer prevents the association of polymer–protein conjugates; (c) after attachment of the polymer to the Ab the former surrounds the surface of the protein globule in a compact manner, and the protein globule strongly affects the structure of the attached polymer, and (d) there is a strong interaction of conjugate with solvent molecules.

The revealed ability of the conjugate to undergo a reversible pH-dependent phase transition from a soluble to an insoluble or colloid state, depending on the nature of the polymer component, is intriguing for understanding protein behavior in the living cell as well as for developing of new bioseparation and bioanalytical methods.

REFERENCES

1. S. V. Kazakov and N. I. Chernova, in *Light Scattering and Photon Correlation Spectroscopy*, E. R. Pike and J. B. Abbis, eds. (Kluwer Academic, Academic, 1997), pp. 401–422.
2. W. Brown (ed.), *Dynamic Light Scattering* (Clarendon, Oxford, 1993).
3. S. E. Harding, D. B. Sattelle, and V. A. Bloomfield (eds.), *Laser Light Scattering in Biochemistry* (Royal Society of Chemistry, London, 1990).
4. W. Burchard, *Adv. Polym. Sci.* **143**:113 (1999).
5. M. B. Dainiak, V. A. Izumrudov, V. I. Muronetz, I. Yu. Galaev, and B. Mattiasson, *Biochim. Biophys. Acta* **1381**:279 (1998).
6. V. I. Muronetz, S. V. Kazakov, V. A. Dainiak, M. B. Izumrudov, I. Yu. Galaev, and B. Mattiasson, *Biochim. Biophys. Acta* **1475**:141 (2000).
7. H. Morawetz, *Macromolecules in Solution* (Wiley, New York, 1965), p. 363.
8. J. Xia and P. Dubin, in *Macromolecular Complexes in Chemistry and Biology,* P. Dubin, J. Bock, R. Davis, D. N. Schulz, and C. Thies, eds. (Springer-Verlag, Berlin, 1994).
9. K. V. Fokina, M. B. Dainyak, N. K. Nagradova, and V. I. Muronetz, *Arch. Biochem. Biophys.* **345**:185 (1997).
10. E. V. Anufrieva, T. M. Birshtein, T. N. Nekrasova, O. B. Ptitsyn, and T. V. Sheveleva, *J. Polym. Sci. Part C* **16**:3519 (1968).
11. S. V. Kazakov, V. I. Muronetz, M. B. Dainiak, V. A. Izumrudov, I. Yu. Galaev, and B. Mattiasson, *Macromol. Biosci.* **1**:157 (2001).
12. Ch. Wu and X. Wang, *Phys. Rev. Lett.* **80**:4092 (1998).